A Cryo-/Liquid Phase Correlative Light Electron Microscopy Workflow to Visualize Crystallization Processes in Graphene Liquid Cells

Luco Rutten, Marit de Beer, Rona Roverts, Anat Akiva, Elena Macías-Sánchez, Nico Sommerdijk**

L Rutten, M de Beer, R Roverts, A Akiva, E Macías-Sánchez, N Sommerdijk
Department of Medical BioSciences, Research Institute for Medical Innovations, Radboud University Medical Center, Geert-Grootplein Zuid 28, 6525 GA Nijmegen, Netherlands
E-mail: elena.macias@ugr.es nico.sommerdijk@radboudumc.nl

L Rutten, M de Beer, R Roverts, A Akiva, E Macías-Sánchez, N Sommerdijk
Electron Microscopy Center, Radboudumc Technology Center Microscopy, Radboud University Medical Center, Geert-Grootplein Noord 29, 6525 EZ Nijmegen, Netherlands

E Macías-Sánchez
Department of Stratigraphy and Palaeontolgy, University of Granada, Avenida Fuente Nueva S/N CP: 18071, Granada, Spain

Keywords: liquid phase transmission electron microscopy, cryo-correlative light electron microscopy, graphene liquid cells, crystallization

Abstract

Liquid phase electron microscopy has emerged as a powerful technique for *in-situ* observation of material formation in liquid. However, the interaction of electrons with an aqueous environment leads to the decomposition of water molecules into multiple radicals (radiolysis), which can affect the formation process. Graphene's ultra-conductive properties have made it an efficient way to mitigate this problem, as it acts as an electron scavenger when used as a window material. However, finding accessible and reliable protocols for the formation of graphene liquid cell (GLC) has been an enormous challenge. Even though loop-assisted transfer has recently been demonstrated as an effective method, the liquid cells are randomly formed and the process of interest is initiated when the GLCs are sealed. This means that the process cannot be imaged at early timepoints, because searching for their location is a time-consuming effort during which the sample is exposed to electrons.

Here we report a novel cryogenic/liquid phase correlative light/electron microscopy workflow that addresses some of the limitations of the graphene liquid cells, combining the advantages of fluorescence and electron microscopy. Fluorescence microscopy (FM) is used to locate the GLCs without exposure to electrons and electron microscopy to capture dynamics with nanoscale resolution. This workflow allows imaging to be initiated at a predetermined space and time by vitrifying and thawing at the moment of interest. We demonstrate the workflow by observing non-classical crystallization pathways, but also highlight its potential application in biological systems.

1. Introduction

A liquid environment is necessary for most synthetic and biological material-forming processes to occur, which often span multiple time (milliseconds to days) and length scales (sub nanometer to micrometer) [1,2]. To properly characterize the mechanism of material formation, it is necessary to gather not only dynamic visual information, but also to combine it with chemical/molecular information[1,3]. Cryo-Transmission Electron Microscopy (cryo-TEM) is the standard technique used to elucidate mechanisms of material development in hydrated conditions[1,4]. By taking snapshots at specific timepoints in the formation process, multiple pathways of material formation have been reconstructed for, among others, biomineralization[5,6], crystallization[7] and self-assembly processes[8]. However, they do not provide information on the dynamics of these processes.

In the last decades, liquid phase electron microscopy (LP-EM) has evolved as a revolutionary technique to provide dynamic real-time, nanoscale imaging in aqueous environments. Developments in both hardware (detectors, phase plates, aberration correctors, etc.) and software (sparse imaging, image processing, radiolysis modeling, etc.) have enabled the *in-situ* observation of material formation with chemical information at high resolution[3,9-13].

However, the interaction of electrons with a liquid layer generates a complex sequence of chemical reactions (radiolysis) resulting in the formation of intermediate species that influence the experimental process[14]. This makes the dose tolerance for both synthetic and biological materials even lower than for other electron microscopy techniques[15]. The use of graphene as encapsulating material has become a way to reduce this problem. Due to its ability to mitigate reactive species, graphene is able to reduce electron damage, thereby increasing the critical electron dose[16]. In addition, its ultrathin structure and electrotransparency significantly increase the resolution compared to standard SiN windows[17,18], enabling the observation of beam sensitive materials with high resolution and contrast[19,20].

However, finding an accessible and reliable method to fabricate graphene liquid cells (GLCs)[21] remains difficult. Loop-assisted transfer (LAT) is often the method of choice to transfer graphene[22-24], but it still involves a highly delicate manual handling where the integrity of graphene is easily lost[25]. But even more important, GLCs randomly formed on the grid, which put additional effort into searching for the location of the GLCs and confirming the presence of liquid under the TEM. Considering that the reaction starts at the moment the cell is sealed, the time lag until visualization implies a serious limitation in accessing to the early reaction stages. In addition, the exposure of the sample to the electron beam when searching for the GLCs in the TEM decreases the number of electrons available for imaging. The ability to localize the

regions of interest (ROIs) without exposing the sample to electrons would therefore increase the amount of information that could be extracted without exceeding the critical dose.

In structural biology, correlative light electron microscopy (CLEM) has become a successful technique for bridging processes occurring at different spatial scales. CLEM uses the large field of view provided by fluorescence microscopy (FM) to localize the ROIs and subsequently image this region at high resolution with EM [26]. In order to preserve the near-native hydrated state[27], the complete workflow can be carried out in cryogenic conditions. Cryo-fixation arrests all processes in a vitreous state, enabling the observation in high resolution cryo-EM, but thereby prohibits the observation of dynamics.

Here, we present a novel workflow which combines the advantages of cryo-CLEM with LP-TEM, correlating TEM and FM in both vitrified and liquefied (fluid) conditions. After graphene encapsulation, the sample is vitrified at a chosen timepoint, which allows localization of the GLCs with Fluorescence microscopy while the reaction is in cryo-arrest. The reaction is then reinitiated by controlled thawing inside the TEM, enabling the real-time dynamic information to be captured at the onset of the reaction. This workflow has proved effective for investigating developmental pathways involved in the nucleation and growth of inorganic crystals, but more importantly, it has enormous potential in visualizing the dynamics of biological processes.

2. Results

The cryo-/LP-CLEM workflow demonstrated here is used to investigate material formation processes. Cryo- and liquid phase TEM are combined to obtain the benefits of both cryo-TEM at a desired time point with the dynamics of LP-TEM. By correlating electron microscopy to fluorescence microscopy, the location of the GLCs on the grid is determined without exposing the sample to electrons.

2.1 Cryo-/LP-CLEM workflow

The workflow consists of two main parts: the graphene liquid cell preparation (Figure 1, top row) and the correlative imaging sequence (Figure 1, bottom row). First, a sample together with a non-reactive fluorescent dye is encapsulated in graphene by automated loop-assisted transfer (aLAT). During the formation of the liquid pockets, the dye is concentrated which enables the localization of the GLCs with FM, and determining the right time for vitrification. Visualization of the grid using cryo-Fluorescence Microscopy (cryo-FM) allows localization of the GLCs without exposing the sample to electrons. Subsequently the grid is transferred to the cryo-TEM, where it is thawed using the temperature controller of the cryo-holder, allowing the dynamics

of the reinitialized process to be captured with LP-TEM. After the experiment, and to certify the stability of the liquid pockets, the grid is imaged with live-FM.

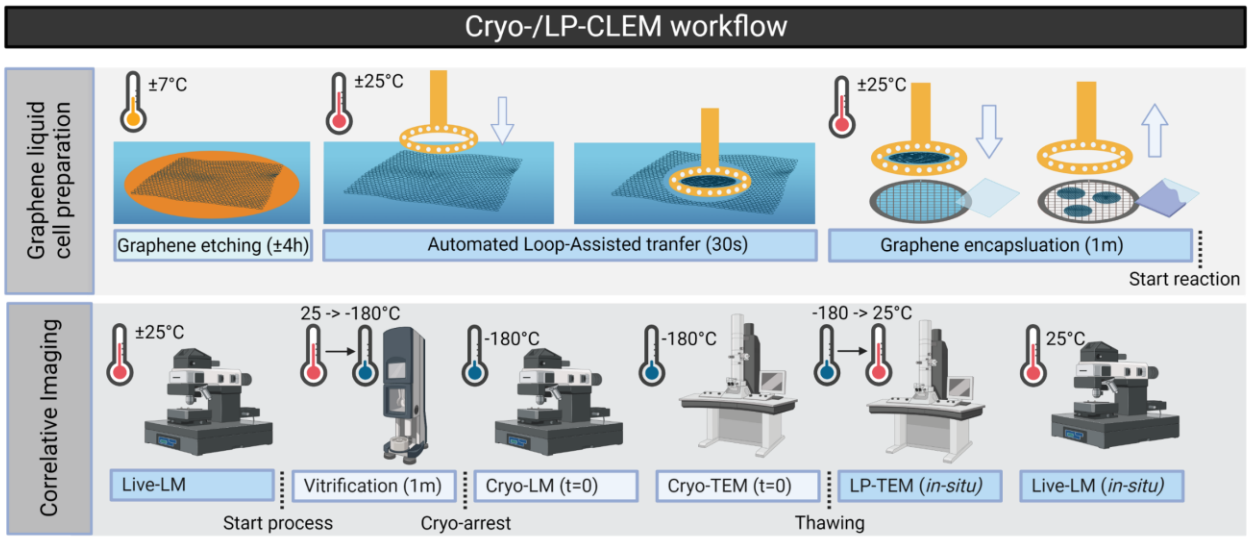

Figure 1. Schematic overview of the cryo-/LP-CLEM workflow. Graphene liquid cell preparation is completely automated. The machine etches away the copper (7°C), transfers the graphene to a TEM grid via loop-assisted transfer and seals the GLCs by blotting away excess liquid. The reaction starts once the liquid pockets are sealed. Live fluorescence microscopy can be used to determine not only the location, but the specific time to image at high resolution, at which point the process is arrested by rapid vitrification. ROIs are located using cryo-fluorescence microscopy and hereafter they are imaged at nanometer resolution (cryo-TEM). The process is reinitiated inside the microscope by heating-up the grid using a cryo-holder, and the reaction dynamics are directly recorded (LP-TEM). To confirm that GLCs remain intact and retain liquid after TEM observation, fluorescence microscopy is used.

To demonstrate the workflow, a crystallization buffer (0.85x PBS, 1.7 mM $CaCl_2$, 9.5 mM K_2HPO_4, 150 µg/mL poly aspartic acid) together with a non-reactive fluorescent dye (CF 680, free acid) was encapsulated in graphene on a finder grid with 4 nm amorphous carbon support film using the aLAT method. The aLAT method showed high yield in both quantity and size of the liquid pockets (Figure 2a). On average each 90 μm x 90 μm grid square contained 89 ± 39 GLCs with 30% being between 0-100,000 nm^2 (0.1 um^2) in area and 10 % of the liquid pockets were larger than 600,000 nm^2 (0.6 um^2) (Figure 2a) which is equivalent to a round liquid pocket with a radius larger than 437 nm. Forty minutes after encapsulation the grid was vitrified to arrest the crystallization process. A cryo-confocal reflection microscopy overview (Figure 2b)

shows the finder grid which was used to correlate the different imaging modalities. The dye, used for evaluating clearance in organs, only emits fluorescence when hydrated. Magenta spots visualized by cryo-FM indicated the location of the liquid pockets on the vitrified grid (Figure 2c). The overlay of low-magnification cryo-TEM images with cryo-FM images (Figure 2d) was used to identify the hydrated liquid pockets (Figure 2d, red square). Other spots which did not show the bright fluorescent signal, were either large hexagonal ice crystals (Figure 2d, circle), not encapsulated crystals, or broken liquid pockets (Figure 2d, dotted circle). Higher resolution cryo-TEM imaging (Figure 2e) showed small (<50 nm) ice crystals spread through the surface of the sample and as well as the bigger crystals (marked with asterisks) that had developed between encapsulation and vitrification. The contrast difference surrounding the crystals marks the outline of the liquid pocket (Figure 2e). The grid was then heated within 45 min from ±176 ^{o} C to room temperature inside the microscope to re-start the reaction, resulting in the evaporation of the surface ice crystals (Figure 2f-g) and the phase transformation from the vitreous ice to liquid water (Figure S1).

The overlay of the live-FM (green) and LP-TEM overview revealed pockets that still contained liquid after thawing (Figure 2f, green areas). Immediately after, no progress in the crystallization is yet observed (Figure 2e, g). However, liquid pockets showing fluorescence in both cryo- and live-FM remained stable for periods of several days to more than a month (Figure S2), allowing us to monitor the crystallization process over a longer time frame. Thawing can also cause rupture of the large liquid cells (< ± 1 µm) (Figure S3). These unstable GLCs cannot be observed without vitrifying the GLCs because after melting of the ice they immediately collapse due to the evaporation of the solution under the high vacuum of the TEM.

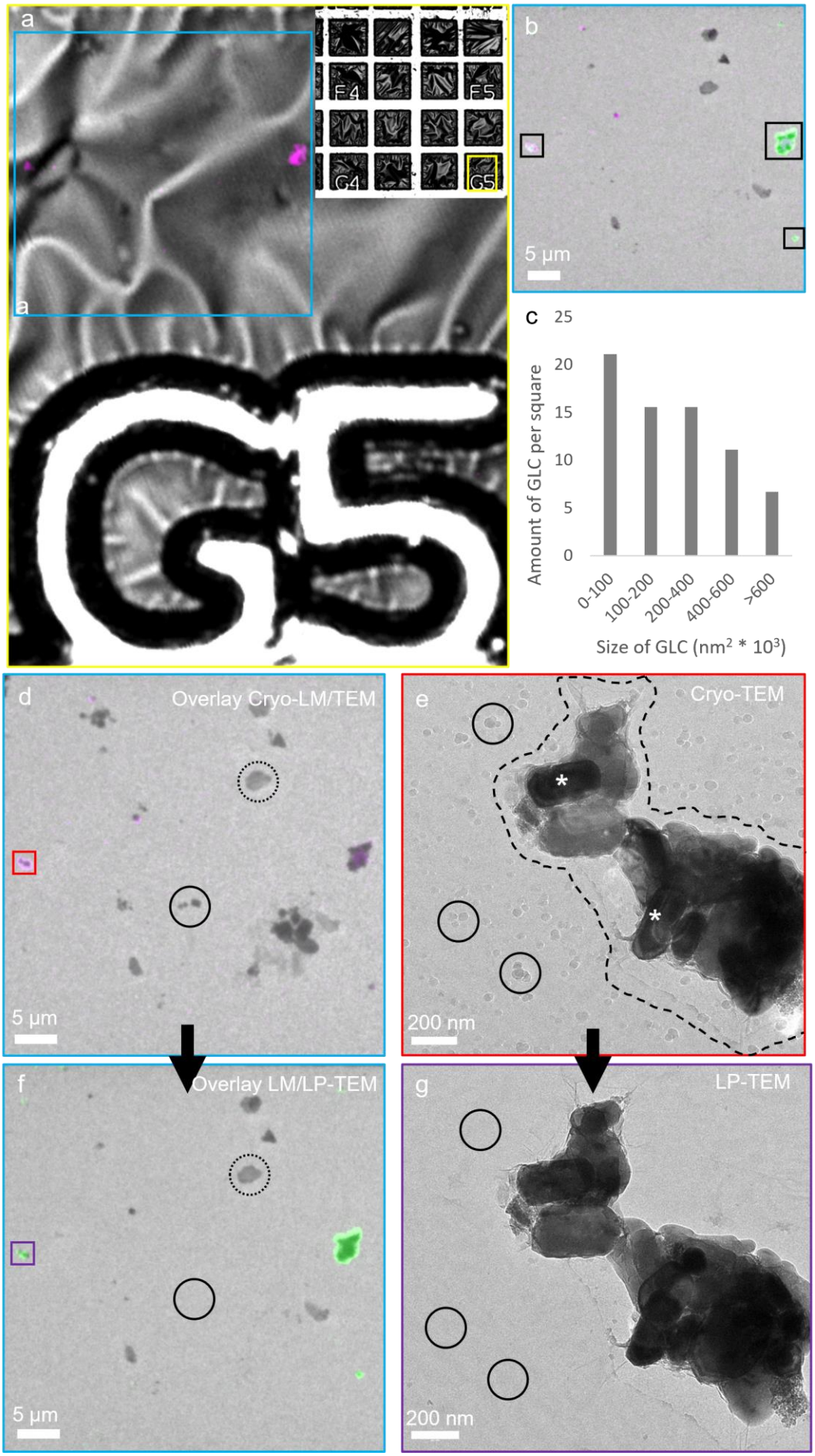
a
F4
F5
G4
G5
b
5 µm
c
Amount of GLC per square
25
20
15
10
5
0
0-100
100-200
200-400
400-600
>600
Size of GLC (nm² * 10³)
d
Overlay Cryo-LM/TEM
5 µm
e
Cryo-TEM
200 nm
f
Overlay LM/LP-TEM
5 µm
g
LP-TEM
200 nm

Figure 2. Correlative cryo-/liquid phase imaging of graphene liquid cells. a) Size distribution of the viable graphene liquid pockets after grid thawing and based on correlation between live-FM and LP-TEM. b) Overview of the vitrified finder grid made with cryo-confocal reflection microscopy showing the position of the area of interest (yellow box). c) Superimposition of the cryo-fluorescence image (magenta) and the confocal reflection microscopy image of the buffer encapsulated in graphene together with the non-reactive dye (magenta). d) Overlay of cryo-TEM with cryo-FM (magenta) of the area indicated by the blue box in Figure 2c. Magenta areas indicate the hydrated pockets (red box). Non-fluorescent higher contrast spots are large ice crystals (circle) or ruptured liquid pockets/contamination (dotted circle). e) High resolution cryo-TEM showing the liquid pocket labeled by the fluorescent signal in Figure 2d (red box). The outline of the liquid pocket is indicated with a dashed line. Circles indicate ice contamination and asterisks the crystals that were formed inside the liquid pockets (total dose 2 $e^-/Å^2$). f) Overlay of LP-TEM with live-FM (green) of the same area (blue box Figure 2a) after thawing the grid inside the microscope. Green areas indicate liquid pockets (purple box). Ice crystals are evaporated (empty black circles) but broken liquid pockets remain (dotted circle). g) High resolution LP-TEM of the liquid pocket indicated with the purple box in Figure 2f (total dose 4 $e^-/Å^2$). Ice crystals that were present in Figure 2e have evaporated (empty black circles).

2.2 Crystallization pathways in GLCs

Observations of the GLC over multiple days have shown various pathways of crystallization. A low magnification LP-TEM overview with live-fluorescence overlay (Figure 3a) confirmed the presence of liquid in the pockets two days after thawing. A high magnification LP-TEM image of a large GLC (inset Figure 3a) and its corresponding diffraction pattern (Figure 3b) show the formation of a large rectangular sodium chloride crystal, which was confirmed by EDX (Figure S4). The diffraction pattern shows bright spots which correspond to sodium chloride crystals (inner circle) or the graphene (outer circle). In addition, blurred rings from the amorphous carbon are also visible in the diffraction pattern. Figure S5 shows a reference diffraction pattern for graphene on top of amorphous carbon without material encapsulation.

Besides these large GLCs, multiple smaller pockets, which vary in size and mineral phase are present (Figure 3c). The crystal in Figure 3d shows two relatively large sodium chloride crystals encapsulated by graphene and surrounded by liquid. A hydrated environment is confirmed by multiple observations: 1) the fluorescent signal[22] (Figure 3a) 2) the outline of the liquid pocket is visible (Figure 3d) 3) the graphene wrinkles around the crystal (Figure 3d) and 4) the crystal is surrounded by an intensity gradient[28] (Figure 3d). Two days after encapsulation two separate crystals are present in the GLCs (Figure 3d). After five days the crystals have merged (Figure 3e) and changes in the external crystal shape or habit are observed (Figure 3f). The crystal habit transformation over multiple days (Figure 3e & Figure 3f) could be attributed to oriented attachment of the two crystals, dissolution/reprecipitation and/or (nano)particle attachment. These transformations of the crystal habit result in tighter encapsulation of the graphene in the lower left side of the crystal associated with a reduced intensity gradient due to the loss of water.
There are also GLCs present in which - based on the shape and the absence of diffraction contrast - an apparently amorphous-like phase was observed which remains present over the next two days. (Figure 3g). After five days, small crystalline domains (based on the diffraction contrast they produce) have nucleated from the amorphous-like phase (Figure 3h). Subsequently, the two crystals have coalesced and transformed into a crystalline state after seven days (Figure 3i). The same observations are made in the small GLCs (Figure 3j). First, nucleation of small crystalline domains from an amorphous phase is visible (Figure 3k) but after three more days the crystal in the top pocket did not grow further but rather dissolved again (Figure 3l). In the bottom GLC the small crystalline domains transform into a stable cubic crystalline phase (Figure 3l). To confirm that the gradient surrounding the GLCs contains

liquid, several GLCs were imaged using a high electron dose (total electron dose > 100 $e^-/Å^2$), which resulted in direct bubbling of the liquid due to radiolysis (Figure S6).

Crystals that are not encapsulated in graphene (i.e. crystals formed before encapsulation) are clearly distinguishable from the crystals inside a GLC because they have clear Fresnel fringes all around them. Besides the absence of a fluorescent signal, there are also no wrinkles, pocket outline or intensity gradient which indicates that the crystal is not encapsulated. Since there is no mineral precursors supply, these crystals (red box Figure 3c) do not show crystal growth, but instead retain their original external shape and size (Figure 3m-o).

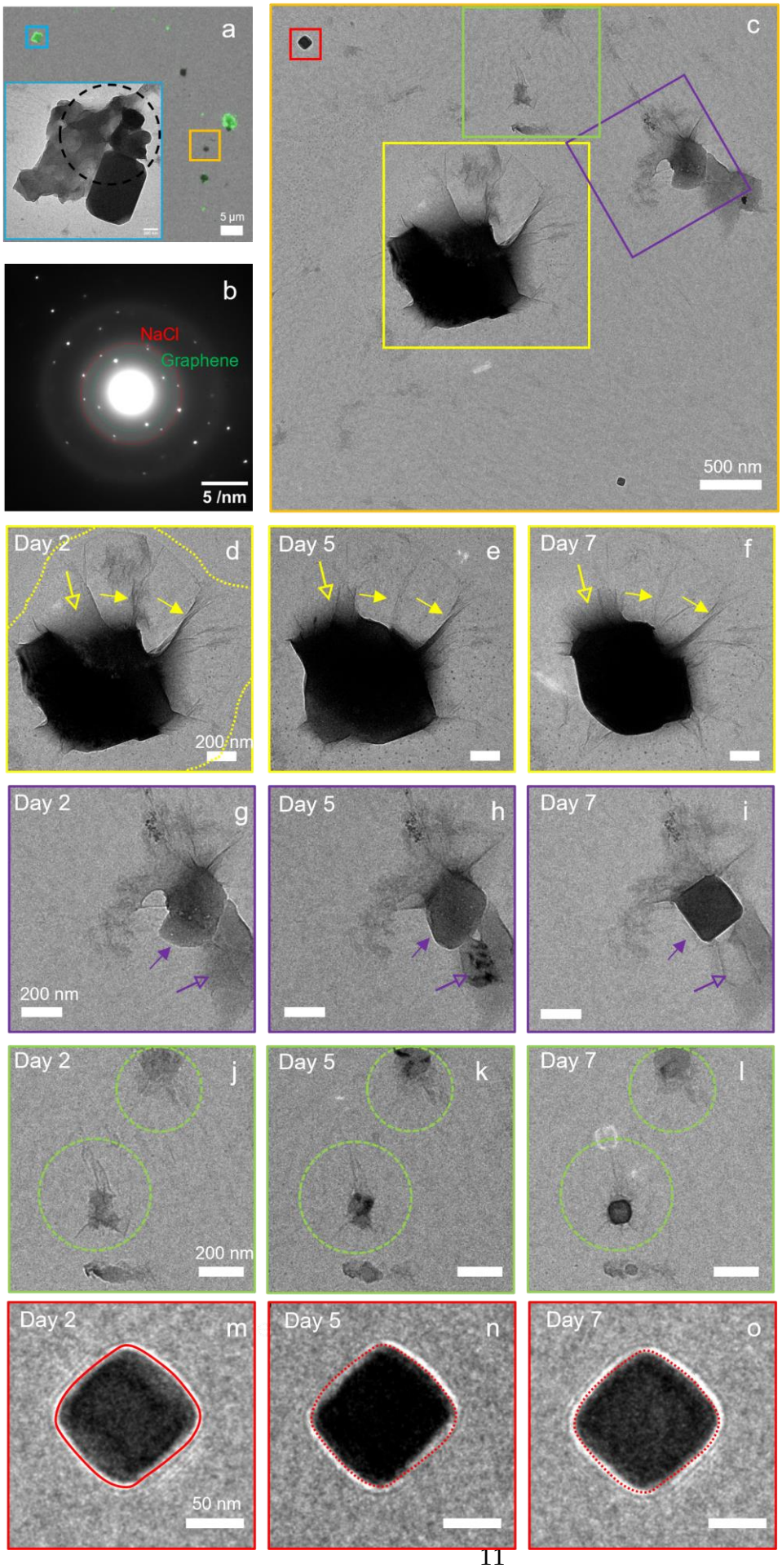
a
5 µm
b
NaCl
Graphene
5 /nm
c
500 nm
Day 2
d
200 nm
Day 5
e
Day 7
f
Day 2
g
200 nm
Day 5
h
Day 7
i
Day 2
j
200 nm
Day 5
k
Day 7
l
Day 2
m
50 nm
Day 5
n
Day 7
o

Figure 3. Cryo-/LP-CLEM workflow to visualize crystallization processes inside a GLC. a) TEM overview imaged two days after thawing, overlaid with live-FM (green) to indicate the GLCs. Insert shows a high magnification LP-TEM image of the GLC in the blue box. b) SAED pattern taken at the position indicated by the black dashed circle in Figure 3a. Inner ring in the DP shows the contribution of the [100] plane on NaCl and outer ring the contribution of the graphene. c) Enlargement of the area marked by the orange box in Figure 3a were multiple GLCs are present (green, yellow and purple boxes) and a crystal that is not encapsulated by graphene (red box). D-f) Large crystal inside a GLC imaged at multiple time points after thawing (3d: 2 days; 3e: 5 days; 3f: 7 days) shows morphological changes. Graphene wrinkles (close yellow arrow), outline of the GLC (dotted yellow line) and the intensity gradient of the liquid surrounding the crystal (open yellow arrow) are visible at all time points. g) Two different but interconnected GLCs imaged two days after thawing (open and closed purple arrows). h) Condensation (solid arrow), and phase transformation (open purple arrow) observed within the pockets five days after thawing. I) Cubic NaCl crystal resulting from an Ostwald ripening process observed seven days after thawing j) Liquid pockets (green dashed circles) containing an amorphous-like phase. k) Nucleation within the amorphous phase contained in the GLCs (green striped circles). l) Dissolution of small crystals (top circle) and further crystallization (bottom circle) inside the GLCs. m) Crystal not encapsulated by graphene outlined by the red dotted line shows only minimum morphological changes five (3n) and seven (3o) days after thawing. Accumulative dose: a) 0.75e^-/Å^2; c, d, g, j, m) 0.15 e^-/Å^2; e, h, k, n) 0.30 e^-/Å^2; f, i, l, o) 0.45 e^-/Å^2

2.3 Crystal migration in a GLC

Besides using the fluorescent signal to tag the liquid pockets in TEM overviews, high resolution FM can also be used to mark the hydrated area in a large pocket. In Figure 4a the overlay of high resolution cryo-FM and cryo-TEM shows multiple connected hydrated areas. After thawing, the GLC remains hydrated and the large crystals in the top left corner are surrounded by liquid (Figure 4b). Some graphene edges are visible in the large GLC which results in compartmentalization of the GLC (Figure 4b, arrowheads).

Directly after thawing, tiny crystals were often observed within the GLCs (Figure 4c, d, f). Multiple events of dissolution (Figure 4d-e) and reprecipitation (Figure 4f-g) or Oswald ripening (Figure 4f, g), which involve the dissolution of small crystals and the redeposition of the dissolved species on the surfaces of the larger ones (Figure 4g) were monitored. In certain

cases we could identify the effect of confinement introduced by the GLC. Some of the facets of the larger crystals did not fully develop due to the growth limitation imposed by the graphene monolayer and appeared truncated (Figure 4h-i). The growth of these large crystals ceased at a certain point (Figure 4h, day 5), although the liquid cell seemed to still contain mineral precursors, judging by the development of small crystals (Figure 4i, day 8).

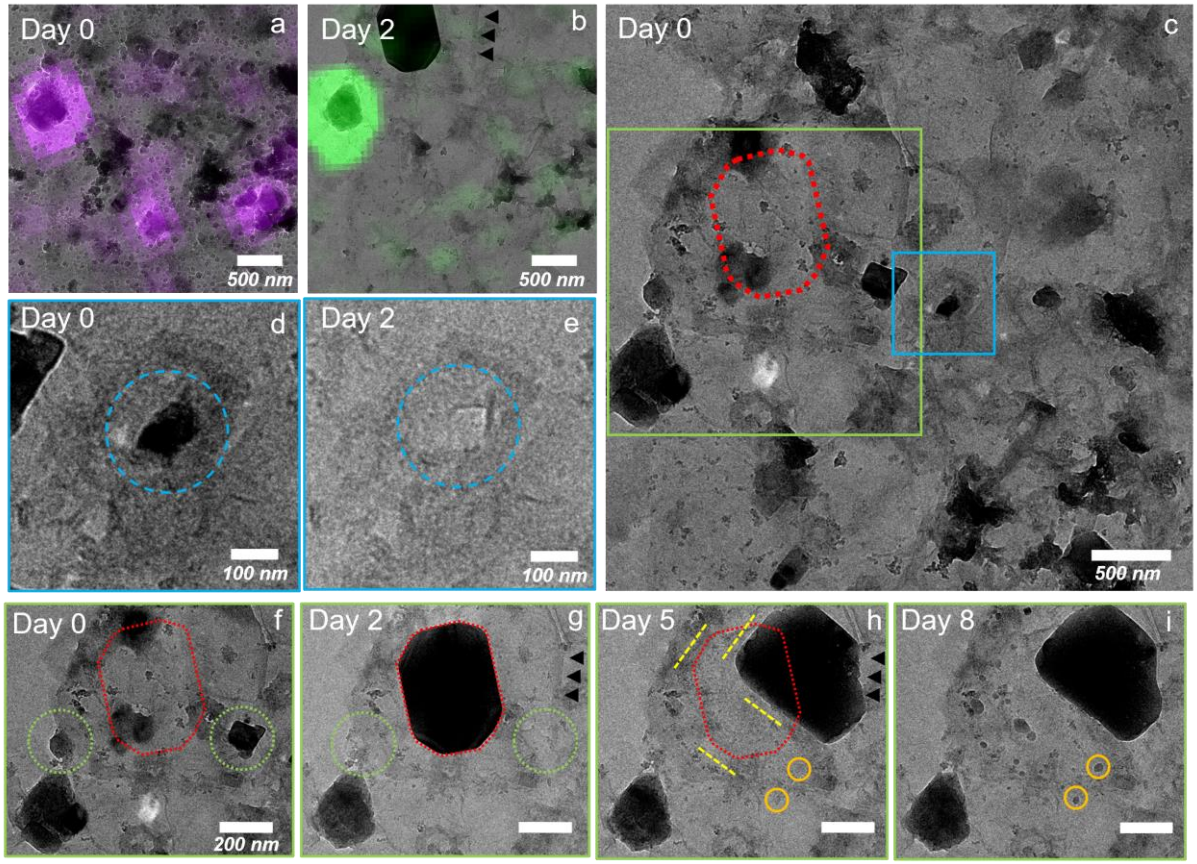

Figure 4. Crystallization processes in a GLC. a) Large GLC in which multiple crystals have already formed in the time between encapsulation and vitrification (correlation between high resolution fluorescent cryo-microscopy (magenta) and cryo-TEM). b) Two days after thawing there is still liquid inside the GLC (correlation between live-fluorescence microscopy (green) and LP-TEM). Edges inside the GLC mark the different compartments inside the GLC (black arrowheads) c) Overview of the GLC directly after thawing. d) Higher magnification image of the area indicated by the blue box in c), showing a crystal formed between encapsulation and vitrification. e) After two days, the crystal in d) has completely dissolved. f) Day 0: Enlarged image of the liquid pocket indicated by the green box in c), directly after thawing. Dotted rounded rectangle indicates the position where a large crystal is formed two days after thawing (g). Crystals within the green dashed circles will dissolve. g) Day 2: Two days after thawing small crystals have dissolved (green dotted circles (f)). Graphene edge (black arrowheads) is visible inside the big GLC. h) Day 5: dissolution and growth of the large crystal in its favorable growth directions (yellow striped lines). The crystal stops growing at the edge of the graphene five days after thawing. Other very small nucleation points are visible (orange circles). i) Day 8: No further growth of the large crystal is observed, but the smaller crystals in the orange circles continue to grow eight days after encapsulation. Accumulative dose: a, d, f) 0.19 $e^-/Å^2$; b, e, g) 0.53 $e^-/Å^2$; c) 0.38 $e^-/Å^2$; h) 0.68 $e^-/Å^2$; i) 0.81 $e^-/Å^2$.

3. Discussion

3.1 Cryo-/LP-CLEM workflow

The correlative approach presented in this paper implements the established correlative cryo-CLEM in a novel cryo-to-LP-TEM approach by thawing the ice in a GLC and thus reinitiating the reaction in the microscope. By using a correlative workflow, the different techniques complement each other, overcoming their inherent limitations[29].

3.1.1. Automated loop-assisted transfer for GLC formation

A reliable method for the transfer and formation of liquid cells formation is essential for LP-TEM experiments. The automated loop-assisted transfer (aLAT) has been shown to outperformed the manual method in both number of cells produced and cell size. aLAT yield approximately a 10x higher amount of GLCs[22], and the size of the liquid cells is higher when compared with manual transfer (ranging from ±100 nm^2 to over 6000000 nm^2). The optimal size of a GLC will ultimately depend on the process of interest. The highest resolution can be obtained in smaller liquid cells, where the liquid layer is minimized. However, when a larger volume is required, bigger GLCs are necessary.

Additionally, the aLAT method offers a high degree of repeatability in terms of the volume of liquid transferred. It should be noted that the initial solution deposited on the grid will mix with the solution transferred by the loop. Since the collection of the graphene is automated, the amount of solution in the loop is consistent (±1 µL), which is an essential parameter for calculating the final concentration of the encapsulated solution that will finally trigger the reaction.

3.1.2. Cryo-correlative light and electron microscopy

Cryo-CLEM studies have shown that a correlative approach is well suited to locate ROIs under cryogenic conditions[30]. However, so far only a few papers have applied the benefits of FM in combination with LP-EM, either to locate water-containing GLCs[12], to confirm the hydrated state of fixated cell after TEM imaging[20] or to investigate electron beam-induced reactions[23]. The use of the cryo-CLEM approach in combination with TEM offers the possibility to locate the GLCs without exposing the sample to electrons. In addition, during the search process the reaction is kept in cryo-arrest, which eliminates the limitations to monitor the earliest stages. Last but not least, it is also a non-destructive method to confirm the hydrated environment. Other frequently applied techniques often require a high electron dose, such as inducing

bubbles[28], or obtaining the energy electron loss spectrum of water[28], which often damage or even destroy the liquid cell.

3.1.3 Correlative cryo- and liquid phase electron microscopy

Time resolved cryo-TEM is used as a complementary technique to LP-TEM by vitrifying at multiple timepoints[31-34]. It does not provide information on the dynamics between these time points, but can be used to benchmark the observations from LP-TEM in terms of electron-beam-induced reactions, confinement, or surface charges[1,35-37].

Recently, microsecond time-resolved cryo-EM has been applied by shortly melting the ice with a laser[38,39]. This allowed the study of fast proteins dynamics under cryogenic conditions and bridges the gap between cryo- and LP-TEM closer together. However, often material formation processes have longer timescales.

Directly correlating the cryo-TEM and LP-TEM provides both the nanoscale resolution in vitreous conditions at predetermined time and the dynamic information. However, to correlate cryo-to-liquid phase microscopy, the liquid must be thin enough to be vitrified properly and thawed without breaking the confinement of the liquid cell. Graphene liquid cells meet these requirement and vitreous ice containing GLC can be produced by plunge freezing the grid in liquid ethane. With the current workflow we demonstrate the ability to reinitialize a reaction by thawing the vitreous sample in the microscope while *in-situ* imaging. The stability of the GLCs allows to observe the dynamic of the reaction for multiple days after thawing and to take the sample back to the fluorescent microscope to confirm the hydrated state of the GLC of interest.

3.1.4. Applications for beam sensitive material formation processes

The advantages of the cryo-/LP-CLEM workflow highlighted in this paper could be beneficial for the observation of complex biological processes, such as enzymatic activity. In addition, fluorescent labelled proteins could be visualized with live fluorescent microscopy and immediately vitrified at a moment of interest[30,40]. This would enable the co-localization of proteins to accurately determine the timepoint of interest for vitrification and subsequent cryo-TEM imaging.

3.2 Crystallization in GLCs

LP-TEM has been used to visualize nucleation and crystal growth[34,41,42]. Atomic resolution can be achieved in liquid when the liquid layer is thin enough, as it is the case with GLCs[43]. However, nucleation is a process that occurs in seconds to minutes[44]. To image a mineralization process for multiple hours or days, as for example in studying process related to biomineralization[6,45], a very stable liquid cell is needed. The described method allowed monitoring of the crystallization process up to eight days after thawing, and some GLC continue to show a fluorescent signal more than one month after thawing, demonstrating the stability of the GLCs and thus the ability to observe reaction for extended periods.

The relatively small size of the liquid pockets enables imaging at high resolution but also limits the reaction volume. Supporting the graphene by encapsulated material or a patterned frame work [46 47] could enlarge the encapsulated volume. Since GLCs are sealed volumes, the absence of flow prevents the ability to change or introduce reactants during the process. The mitigation of these limitations could involve the design of liquid-flowing graphene chips[53] that allow the vitrification and correlation of fluorescence microscopy to cryo/LPEM.

Our observations indicate the occurrence of multiple parallel (non)classical crystallization pathways such as amorphous-phase-mediated crystallization, oriented attachment, particle aggregation or Ostwald ripening and nanoparticle attachment[48-50]. Although the characterization of the different crystallization pathways is beyond the scope of this study, we believe that the cryo/LPEM workflow provides a means to control the crystallization environment while allowing for high resolution imaging, providing the perfect platform to investigate crystallization processes.

Nevertheless we note that the use of GLCs can influence the observed nucleation and growth processes. The surface to volume ratio in GLC is enormous compared to bulk reaction. Heterogeneous nucleation could occur at the liquid/graphene interface even though these interface reactions are expected to be smaller at low atomic number materials[37]. Second, the cascade of reactions which occur when the beam interacts with the aqueous buffer solution will also influence the crystallization[37,51]. Besides, multiple ionic species are already present in the liquid next to the sodium and chloride ions. These impurities are known to influence the growth rate[52,53]. Third, organic macromolecule can stabilize an amorphous phase which influence the rate of nucleation of these meta-stable phases[42,43,45,49]. Crystal domains can nucleate from these amorphous particles and eventually form crystals.

4. Conclusion

In summary, the cryo-/LP-CLEM workflow presented here allows for the observation of material formation processes in high resolution by using graphene as window material. The workflow combines the benefits of cryo-TEM and LP-TEM to be able to image at determined time and space point by vitrifying and reinitiating at the moment of interest. The amount of time necessary for searching the randomly formed GLCs is drastically reduced by combining cryo-TEM with cryo-FM to locate the GLCs. In addition, no electrons are used for searching the GLCs which makes this workflow suitable for beam sensitive processes. The ability to tag a protein with a fluorescent marker, vitrify it and reinitiate the reaction by minimizing the electron dose will certainly benefit the dynamic imaging of biological materials.

5. Experimental Section/Methods

Graphene encapsulation: Gold 200 mesh ultrathin carbon film finder grids were encapsulated with graphene by automated loop-transfer using a Naiad-1 system (VitroTEM, Delft, The Netherlands). Cupper chips coated with graphene by CVD were acquired (VitroTEM, Delft, The Netherlands) and placed inside a Naiad-1 (VitroTEM, Delft, The Netherlands). The machine etches away the cupper with 0.2 M ammonium persulfate and washes the graphene with Milli-Q. After washing the Milli-Q is replaced with the crystallization buffer (0.85x PBS, 1.7 mM $CaCl_2$, 9.5 mM K_2HPO_4, 150 µg/mL poly aspartic acid). A finder grid is placed in the machine and a 3 µL droplet of crystallization buffer with 100x diluted CF®680 dye (Biotium, Fremont, CA, USA) is added on the grid. The graphene is transferred together with the crystallization buffer by automated assisted loop transfer to the grid and the excess liquid is blotted away, which results in the sealing of the liquid pockets.

Cryo-LSM: Encapsulated grids were vitrified by plunge freezing in liquid ethane using a Vitrobot Mark IV (Thermo Fisher Scientific, Eindhoven, The Netherlands) at room temperature. After vitrification, the TEM grids were loaded into a universal TEM cryo-holder (349559-8100-010) using the ZEISS Correlative Cryo Workflow solution, which fit into the PrepDek® (PP3010Z, Quorum technologies, Laughton, UK). The universal cryo-holder containing the samples was transferred into the Linkam adapter to fit the LM cryo-stage (CMS-196, Linkam scientific inc.), which was used with an upright confocal laser scanning microscopy (LSM 900, Zeiss microscopy GmbH) equipped with an Airyscan 2 detector.

Reflection microscopy and fluorescence microscopy were recorded in three different resolution steps. First, overview images at low resolution were made (C Epiplan-Apochromat 5x/0.2 DIC, Zeiss; pixel size 520 nm) using reflection microscopy (0.02% 640nm laser with 500V master gain; Detection 549 - 700) and fluorescence microscopy (4% 640nm laser with 900V master gain; Detection 450 - 700), to visualize the TEM grid bars and liquid pockets, respectively. Next, medium resolution images (C Epiplan-Apochromat 10x/0.4 DIC; pixel size x-y: 195nm) were recorded from regions of interest (ROIs), on various areas of the grid, with the same excitation/emission settings as for the low resolution. Finally, the ROIs were recorded at high resolution (C Epiplan-Neofluar 100x/0.75 DIC; pixel size x-y: 104nm). Settings had to be adjusted for this 100x objective (Reflection microscopy: 0.2% 640nm laser with 500V master gain; Detection 549 – 700 and Fluorescence microscopy: 5% 640nm laser with 950V master gain; Detection 450 - 700). All the fluorescent images were recorded in the super resolution mode and were processed afterwards using the auto filter in Zen Blue. The images were displayed in Zen connect, a plugin in Zen blue (Zeiss system software). Within this program, all the recorded images are stored with its coordinate, allowing navigation with high resolution objectives.

Live-FM: The Zen connect file was opened which stored the previous recorded cryo LM images. The grid was placed on an objective glass and imaged with an upright confocal laser scanning microscopy (LSM 900, Zeiss microscopy GmbH) equipped with an Airyscan 2 detector. The images were recorded in three different resolution steps. First, an overview image at low resolution was made C Epiplan-Apochromat 5x/0.2 DIC, Zeiss; pixel size 624 nm) using reflection microscopy (0.02% 640nm laser with 550V master gain; Detection 549 - 700) and fluorescence microscopy (2% 640nm laser with 900V master gain; Detection 450 - 700). This image was used to align previous cryo-session for easy navigation to the ROIs images with high resolution in cryo. Next, a medium resolution was recorded from the ROIs (C Epiplan-Apochromat 10x/0.4 DIC; pixel size x-y: 195nm), followed by a higher resolution image of each ROI (Plan-Apochromat 20x/0.8 M27, Zeiss; Pixel size 98nm). The setting for the medium and higher resolution were the same as for the low resolution. All the fluorescent images were recorded in the super resolution mode and were processed afterwards using the auto filter in Zen Blue.

Cryo-/LP-TEM imaging: Images were acquired with a JEOL JEM 2100 (Jeol Ltd., Tokyo, Japan) equipped with a Gatan 890 Ultrascan (Pleasanton, CA, USA) and LaB_6 filament

operated at 200 kV using low dose software (Serial EM). EDX mapping was performed with a JEOL JEM 1400 (Jeol Ltd., Tokyo, Japan) equipped with a JED2300T (Jeol Ltd., Tokyo, Japan) and Tungsten filament operated at 60 kV.

Heating-up: Vitrified grids were placed inside a Gatan 914 high tilt cryo-holder (Pleasanton, CA, USA). The liquid nitrogen was removed from cryo-transfer holder without removing the holder form the microscope. The temperature controller unit was used to heat-up the tip of the holder (0.75 mA) in approximately 45 minutes to room temperature.

Acknowledgements

LR, MdB, AA, RR and NS are supported by the European Research Council (ERC) Advanced Investigator grant (H2020-ERC-2017-ADV-788982-COLMIN). EMS is supported by Marie Curie Individual Fellowship, MSCA-IF-2020 DYNAMIN (101031624) and Research Program Juan de la Cierva Incorporación (IJC2020-043639-I) funded by MCIN/AEI/10.13039/501100011033 and European Union NextGenerationEU/PRTR.

References

1 De Yoreo, J. J. & N. A. J. M, S. Investigating materials formation with liquid-phase and cryogenic TEM. *Nature Reviews Materials* **1**, doi:10.1038/natrevmats.2016.35 (2016).

2 Nudelman, F. & Sommerdijk, N. A. Biomineralization as an inspiration for materials chemistry. *Angew Chem Int Ed Engl* **51**, 6582-6596, doi:10.1002/anie.201106715 (2012).

3 Wu, H., Friedrich, H., Patterson, J. P., Sommerdijk, N. & de Jonge, N. Liquid-Phase Electron Microscopy for Soft Matter Science and Biology. *Adv Mater* **32**, e2001582, doi:10.1002/adma.202001582 (2020).

4 Patterson, J. P., Xu, Y., Moradi, M. A., Sommerdijk, N. & Friedrich, H. CryoTEM as an Advanced Analytical Tool for Materials Chemists. *Acc Chem Res* **50**, 1495-1501, doi:10.1021/acs.accounts.7b00107 (2017).

5 Pouget, E. M. *et al.* The Initial Stages of Template-Controlled CaCO3 Formation Revealed by Cryo-TEM. *Science* **323**, 1455-1458, doi:10.1126/science.1169434 (2009).

6 Nudelman, F. *et al.* The role of collagen in bone apatite formation in the presence of hydroxyapatite nucleation inhibitors. *Nature Materials* **9**, 1004-1009, doi:10.1038/nmat2875 (2010).

7 Houben, L., Weissman, H., Wolf, S. G. & Rybtchinski, B. A mechanism of ferritin crystallization revealed by cryo-STEM tomography. *Nature* **579**, 540-543, doi:10.1038/s41586-020-2104-4 (2020).

8 Tidhar, Y., Weissman, H., Tworowski, D. & Rybtchinski, B. Mechanism of Crystalline Self-Assembly in Aqueous Medium: A Combined Cryo-TEM/Kinetic Study. *Chemistry – A European Journal* **20**, 10332-10342, doi:https://doi.org/10.1002/chem.201402096 (2014).

9 Gnanasekaran, K. *et al.* Dipeptide Nanostructure Assembly and Dynamics via in Situ Liquid-Phase Electron Microscopy. *ACS Nano* **15**, 16542-16551, doi:10.1021/acsnano.1c06130 (2021).
10 Mirsaidov, U., Patterson, J. P. & Zheng, H. Liquid phase transmission electron microscopy for imaging of nanoscale processes in solution. *MRS Bulletin* **45**, 704-712, doi:10.1557/mrs.2020.222 (2020).
11 Smith, J. W. & Chen, Q. Liquid-phase electron microscopy imaging of cellular and biomolecular systems. *J Mater Chem B* **8**, 8490-8506, doi:10.1039/d0tb01300e (2020).
12 Danev, R. & Baumeister, W. Expanding the boundaries of cryo-EM with phase plates. *Curr Opin Struct Biol* **46**, 87-94, doi:10.1016/j.sbi.2017.06.006 (2017).
13 Stevens, A., Yang, H., Carin, L., Arslan, I. & Browning, N. D. The potential for Bayesian compressive sensing to significantly reduce electron dose in high-resolution STEM images. *Microscopy (Oxf)* **63**, 41-51, doi:10.1093/jmicro/dft042 (2014).
14 Schneider, N. M. *et al.* Electron–Water Interactions and Implications for Liquid Cell Electron Microscopy. *The Journal of Physical Chemistry C* **118**, 22373-22382, doi:10.1021/jp507400n (2014).
15 Peckys, D. B., Macías-Sánchez, E. & de Jonge, N. Liquid phase electron microscopy of biological specimens. *MRS Bulletin* **45**, 754-760, doi:10.1557/mrs.2020.225 (2020).
16 Cho, H. *et al.* The Use of Graphene and Its Derivatives for Liquid-Phase Transmission Electron Microscopy of Radiation-Sensitive Specimens. *Nano Lett* **17**, 414-420, doi:10.1021/acs.nanolett.6b04383 (2017).
17 Keskin, S. & de Jonge, N. Reduced Radiation Damage in Transmission Electron Microscopy of Proteins in Graphene Liquid Cells. *Nano Lett* **18**, 7435-7440, doi:10.1021/acs.nanolett.8b02490 (2018).
18 Park, J. *et al.* Graphene Liquid Cell Electron Microscopy: Progress, Applications, and Perspectives. *ACS Nano* **15**, 288-308, doi:10.1021/acsnano.0c10229 (2021).
19 Koo, K., Dae, K. S., Hahn, Y. K. & Yuk, J. M. Live Cell Electron Microscopy Using Graphene Veils. *Nano Lett* **20**, 4708-4713, doi:10.1021/acs.nanolett.0c00715 (2020).
20 Park, J. *et al.* Direct Observation of Wet Biological Samples by Graphene Liquid Cell Transmission Electron Microscopy. *Nano Lett* **15**, 4737-4744, doi:10.1021/acs.nanolett.5b01636 (2015).
21 Ghodsi, S. M., Megaridis, C. M., Shahbazian‐Yassar, R. & Shokuhfar, T. Advances in Graphene‐Based Liquid Cell Electron Microscopy: Working Principles, Opportunities, and Challenges. *Small Methods* **3**, doi:10.1002/smtd.201900026 (2019).
22 Deursen, P. M. G. *et al.* Graphene Liquid Cells Assembled through Loop‐Assisted Transfer Method and Located with Correlated Light‐Electron Microscopy. *Advanced Functional Materials* **30**, doi:10.1002/adfm.201904468 (2020).
23 Wang, C., Qiao, Q., Shokuhfar, T. & Klie, R. F. High-resolution electron microscopy and spectroscopy of ferritin in biocompatible graphene liquid cells and graphene sandwiches. *Adv Mater* **26**, 3410-3414, doi:10.1002/adma.201306069 (2014).
24 Wierman, J. L., Alden, J. S., Kim, C. U., McEuen, P. L. & Gruner, S. M. Graphene as a protein crystal mounting material to reduce background scatter. *J Appl Crystallogr* **46**, 1501-1507, doi:10.1107/S002188981301786X (2013).
25 Textor, M. & De Jonge, N. Strategies for Preparing Graphene Liquid Cells for Transmission Electron Microscopy. *Nano Lett.* **18**, 3313-3321 (2018).
26 de Boer, P., Hoogenboom, J. P. & Giepmans, B. N. Correlated light and electron microscopy: ultrastructure lights up! *Nat Methods* **12**, 503-513, doi:10.1038/nmeth.3400 (2015).

27 Kaufmann, R., Hagen, C. & Grunewald, K. Fluorescence cryo-microscopy: current challenges and prospects. *Curr Opin Chem Biol* **20**, 86-91, doi:10.1016/j.cbpa.2014.05.007 (2014).
28 Keskin, S., Pawell, C. & de Jonge, N. Verification of water presence in graphene liquid cells. *Micron* **149**, 103109, doi:10.1016/j.micron.2021.103109 (2021).
29 Chandler, D. E. & Roberson, R. W. *Bioimaging : current concepts in light and electron microscopy*. (Jones and Bartlett Publishers, 2009).
30 de Beer, M. *et al.* Visualizing Biological Tissues: A Multiscale Workflow from Live Imaging to 3D Cryo-CLEM. *Microscopy and Microanalysis* **27**, 11-12, doi:10.1017/s1431927621013635 (2021).
31 Park, H. *et al.* Early Stage Li Plating by Liquid Phase and Cryogenic Transmission Electron Microscopy. *ACS Energy Letters* **8**, 715-721, doi:10.1021/acsenergylett.2c02387 (2022).
32 Peng, X. *et al.* Observation of formation and local structures of metal-organic layers via complementary electron microscopy techniques. *Nat Commun* **13**, 5197, doi:10.1038/s41467-022-32330-z (2022).
33 Zachman, M. J., de Jonge, N., Fischer, R., Jungjohann, K. L. & Perea, D. E. Cryogenic specimens for nanoscale characterization of solid–liquid interfaces. *MRS Bulletin* **44**, 949-955, doi:10.1557/mrs.2019.289 (2019).
34 Zhu, G. *et al.* Self-similar mesocrystals form via interface-driven nucleation and assembly. *Nature* **590**, 416-422, doi:10.1038/s41586-021-03300-0 (2021).
35 Parent, L. R. *et al.* Tackling the Challenges of Dynamic Experiments Using Liquid-Cell Transmission Electron Microscopy. *Acc Chem Res* **51**, 3-11, doi:10.1021/acs.accounts.7b00331 (2018).
36 Ilett, M. *et al.* Evaluation of correlated studies using liquid cell and cryo-transmission electron microscopy: Hydration of calcium sulphate and the phase transformation pathways of bassanite to gypsum. *J Microsc* **288**, 155-168, doi:10.1111/jmi.13102 (2022).
37 Woehl, T. J. Metal Nanocrystal Formation during Liquid Phase Transmission Electron Microscopy: Thermodynamics and Kinetics of Precursor Conversion, Nucleation, and Growth. *Chemistry of Materials* **32**, 7569-7581, doi:10.1021/acs.chemmater.0c01360 (2020).
38 Voss, J. M., Harder, O. F., Olshin, P. K., Drabbels, M. & Lorenz, U. J. Rapid melting and revitrification as an approach to microsecond time-resolved cryo-electron microscopy. *Chemical Physics Letters* **778**, doi:10.1016/j.cplett.2021.138812 (2021).
39 Bongiovanni, G., Harder, O. F., Drabbels, M. & Lorenz, U. J. Microsecond melting and revitrification of cryo samples with a correlative light-electron microscopy approach. *Front Mol Biosci* **9**, 1044509, doi:10.3389/fmolb.2022.1044509 (2022).
40 Heiligenstein, X. *et al.* in *Methods in Cell Biology* Vol. 162 (eds Thomas Müller-Reichert & Paul Verkade) 115-149 (Academic Press, 2021).
41 Wang, X., Yang, J., Andrei, C. M., Soleymani, L. & Grandfield, K. Biomineralization of calcium phosphate revealed by in situ liquid-phase electron microscopy. *Communications Chemistry* **1**, doi:10.1038/s42004-018-0081-4 (2018).
42 Smeets, P. J., Cho, K. R., Kempen, R. G., Sommerdijk, N. A. & De Yoreo, J. J. Calcium carbonate nucleation driven by ion binding in a biomimetic matrix revealed by in situ electron microscopy. *Nat Mater* **14**, 394-399, doi:10.1038/nmat4193 (2015).
43 Yang, J. *et al.* Amorphous-Phase-Mediated Crystallization of Ni Nanocrystals Revealed by High-Resolution Liquid-Phase Electron Microscopy. *J Am Chem Soc* **141**, 763-768, doi:10.1021/jacs.8b11972 (2019).

44 Thanh, N. T. K., Maclean, N. & Mahiddine, S. Mechanisms of Nucleation and Growth of Nanoparticles in Solution. *Chemical Reviews* **114**, 7610-7630, doi:10.1021/cr400544s (2014).
45 Ramnarain, V. *et al.* Monitoring of CaCO(3) Nanoscale Structuration through Real-Time Liquid Phase Transmission Electron Microscopy and Hyperpolarized NMR. *J Am Chem Soc* **144**, 15236-15251, doi:10.1021/jacs.2c05731 (2022).
46 Noh, N. *et al.* Lithographically patterned well-type graphene liquid cells with rational designs. *Lab Chip* **20**, 2796-2803, doi:10.1039/d0lc00440e (2020).
47 Kelly, D. J. *et al.* Nanometer Resolution Elemental Mapping in Graphene-Based TEM Liquid Cells. *Nano Lett* **18**, 1168-1174, doi:10.1021/acs.nanolett.7b04713 (2018).
48 De Yoreo, J. J., Nakouzi, E., Jin, B., Chun, J. & Mundy, C. J. Spiers Memorial Lecture: Assembly-based pathways of crystallization. *Faraday Discuss* **235**, 9-35, doi:10.1039/d2fd00061j (2022).
49 De Yoreo, J. J. In-situ liquid phase TEM observations of nucleation and growth processes. *Progress in Crystal Growth and Characterization of Materials* **62**, 69-88, doi:10.1016/j.pcrysgrow.2016.04.003 (2016).
50 Tao, J., Nielsen, M. H. & De Yoreo, J. J. Nucleation and phase transformation pathways in electrolyte solutions investigated by in situ microscopy techniques. *Current Opinion in Colloid & Interface Science* **34**, 74-88, doi:10.1016/j.cocis.2018.04.002 (2018).
51 Taherkhani, M., Fritsch, B., Jank, M. P. M., Spiecker, E. & Hutzler, A. Modelling the Radiolysis of Silver Nitrate Solutions in presence of Bromide Ions in Liquid-Phase Transmission Electron Microscopy. *Microscopy and Microanalysis* **27**, 103-104, doi:10.1017/s1431927621013519 (2021).
52 Zhu, G., Reiner, H., Colfen, H. & De Yoreo, J. J. Addressing some of the technical challenges associated with liquid phase S/TEM studies of particle nucleation, growth and assembly. *Micron* **118**, 35-42, doi:10.1016/j.micron.2018.12.001 (2019).
53 Liu, Z. *et al.* Shape-preserving amorphous-to-crystalline transformation of CaCO(3) revealed by in situ TEM. *Proc Natl Acad Sci U S A* **117**, 3397-3404, doi:10.1073/pnas.1914813117 (2020).